Electric field tuning of phase separation in manganite thin films

James Lourembam,[1] Jianchun Wu,[2] Junfeng Ding,[3] Weinan Lin,[1] and Tom Wu[3,*]

[1]*Division of Physics and Applied Physics, School of Physical and Mathematical Sciences, Nanyang Technological University, Singapore 637371, Singapore*

[2]*Key Laboratory of Radiation Physics and Technology, Ministry of Education, Institute of Nuclear Science and Technology, Sichuan University, Chengdu 610064, China*

[3]*Materials Sciences and Engineering, King Abdullah University of Science and Technology, Thuwal 23955-6900, Saudi Arabia*

(Received 26 August 2013; revised manuscript received 9 November 2013; published 29 January 2014)

In this paper, we investigate the electric field effect on epitaxial $Pr_{0.65}(Ca_{0.75}Sr_{0.25})_{0.35}MnO_3$ thin films in electric double-layer transistors. Different from the conventional transistors with semiconducting channels, the sub(micrometer)-scale phase separation in the manganite channels is expected to result in inhomogeneous distribution of mobile carriers and local enhancement of electric field. The field effect is much larger in the low-temperature phase separation region compared to that in the high-temperature polaron transport region. Further enhancement of electroresistance is achieved by applying a magnetic field, and a 250% modulation of resistance is observed at 80 K, equivalent to an increase of the ferromagnetic metallic phase fraction by 0.51%, as estimated by the general effective medium model. Our results illustrate the complementary nature of electric and magnetic field effects in phase-separated manganites, providing insights on such novel electronic devices based on complex oxides.

DOI: 10.1103/PhysRevB.89.014425 PACS number(s): 75.70.Ak, 73.50.−h

I. INTRODUCTION

Manipulating the electronic and magnetic phases in correlated electron systems is a promising approach towards novel field-effect switching and nonvolatile memory devices [1–4]. In particular, mixed-valence manganites exhibit a rich variety of electronic and magnetic phases that often coexist and compete with one another [5–9]. Strong correlations among charge, spin, orbital, and lattice are the most cited mechanisms underlying the observed extraordinary physical phenomena, in particular, colossal magnetoresistance (CMR) [10–14]. It is well recognized that many mixed-valence manganites exhibit phase separation between the ferromagnetic (FM) metallic phase and the charge-ordered (CO) insulating phase. When driven by quenched disorders near first-order transitions, the scale of phase-separated domains can reach (sub)micrometers [15–20]. Furthermore, the fraction of the competing phases can be modulated using external parameters like a magnetic field, an electrical field, light, and temperature. Elucidating the competition between the energetically degenerate phases is crucial to harnessing macroscopic properties such as CMR and metal-insulator transition in such complex materials. Although manganites have been intensively studied for several decades, new insights continue to emerge on the characteristics and the dynamic evolution of magnetic domains [21–23], shedding light on the complex behaviors of competing phases in strongly correlated electron systems.

Since carrier density is one of the key parameters controlling the ground state of manganites, there has been a lot of interest in using the electric field effect to electrostatically modulate the physical properties of manganite thin films [24–35]. Unlike the chemical doping, the electric field approach is considered "clean" because it generally does not introduce impurities or extra scattering centers. Besides gaining new understanding and control of the different phases in manganites, such investigations are expected to advance the development of oxide-based electronic devices [36]. There have been several attempts in this research direction. In particular, field effect devices with "all perovskite structures" were fabricated with manganites as the semiconducting channel and dielectrics/ferroelectrics as the gate oxide [24,27,28,37–41]. In the ferroelectric field effect devices, two discrete polarization states of the ferroelectric layers are used to achieve nonvolatile modulation of the channel resistance. Hong *et al*. found a twofold change of resistivity and a shift of 35 K of the Currie temperature in $La_{1-x}Sr_xMnO_3$ (LSMO, $x = 0.2$) films induced by the switching of the $Pb(Zr_xTi_{1-x})O_3$ polarization [24]. Since the carrier density of homogeneous double-exchange LSMO is quite high, the field effect is limited by the Thomas-Fermi screening length of 0.2–0.3 nm [28]. Recently, the electronic origin of charge modulation in these multiferroic structures was probed by Vaz *et al*. [30] using near-edge x-ray absorption spectroscopy, and the paper revealed a field-induced change in the valence state of Mn, which is accompanied by a modified interfacial spin configuration.

Lately, the electric double-layer transistor (EDLT) has emerged as a powerful technique to investigate the electric field effect in a wide range of materials [42–57]. With ionic liquids or electrolytes as the gate dielectric materials, very high electric fields can be sustained before breakdown occurs, and the resulting charge modulation is on the order of 10^{14}–10^{15} cm^{-2}. Using this technique, electrostatic control of the Mott transition [33,34,53,55,58,59] and superconductivity [42,43,51,60] has been reported. The first experiment of using manganite channels in EDLT was carried out by Dhoot *et al*. in 2009 [33]. With 5-nm thin films of $La_{0.8}Ca_{0.2}MnO_3$ as the channel, very large resistance modulations of several orders of magnitude were observed for the positive gate bias, whereas the negative bias produced a much smaller effect [33]. In a recent paper, Xiang *et al*. [34] managed to modulate the conductivity of electron-doped $Ca_{1-x}Ce_xMnO_3$ thin films by

*Corresponding author: tao.wu@kaust.edu.sa

as much as 120 000% by applying a positive bias to the ionic liquid gate. In contrast to the ferroelectric field effect devices, where the inverse piezoelectric effect is entangled with the electrostatic modulation [61–63], strain effect is negligible in EDLT experiments.

In this paper, we present transport studies on EDLT using a strongly phase-separated manganite $Pr_{0.65}(Ca_{0.75}Sr_{0.25})_{0.35}MnO_3$ (PCSMO) as the channel. In the phase diagram of $Pr_{0.65}(Ca_ySr_{1-y})_{0.35}MnO_3$, as y changes from 0.8 to 0.6, the overall physical property transforms from a CO insulator to a FM metal [64]. It has been established that PCSMO exhibits mesoscopic phase separation with (sub)micrometer-sized domains over a range of temperatures [64–71]. Although there have been some studies on EDLT with manganite thin films as channels [33,34], there has been no report so far on using EDLT to explore the field effect on strongly phase-separated manganites like PCSMO. The central theme of this paper is to examine the electric field effect on the competing electronic/magnetic phases in PCSMO and to shed light on the underlying physics. Our results revealed that the electric field modulation on the small polaron transport at high temperatures is rather weak, whereas the field effect is significantly enhanced whenever the system is driven into the phase-separation regime by temperature, a magnetic field, or both. The maximum modulation of resistance reaches 250% at 80 K, corresponding to a 0.51% increase of the FM metallic phase as estimated using the general effective medium (GEM) theory.

II. EXPERIMENTAL DETAILS

PCSMO films were grown on (001) $(LaAlO_3)_{0.3}$-$(Sr_2AlTaO_6)_{0.7}$ (LSAT, cubic structure with $a = 3.87$ Å) substrates using pulsed laser deposition (PLD). The growth temperature was 770 °C, and the oxygen pressure was 40 Pa. After the deposition, the films were annealed for 20 min at the growth temperature under an oxygen pressure of 1000 Pa and then slowly cooled down to room temperature. Bulk PCSMO has an orthorhombic crystal structure with the *Pnma* symmetry, and its lattice parameters $a = 5.445$ (or $3.851 \times \sqrt{2}$) Å, $b = 7.680$ (or 3.840×2) Å, and $c = 5.441$ (or $3.848 \times \sqrt{2}$) Å. Since the lattice mismatch between the film and the substrate is smaller than 1%, in this paper, we ignore the small lattice anisotropy of PCSMO and consider it as pseudocubic.

We systematically grew PCSMO films of various thicknesses from 10 to 100 nm and characterized their transport properties. On the one hand, the electric field effect is usually larger in thinner channels. On the other hand, very thin PCSMO films become too resistive and their magnetic properties degrade. Considering this tradeoff, we carried out device fabrication and measurement using films with a thickness of 30 nm. The structure of the films was characterized

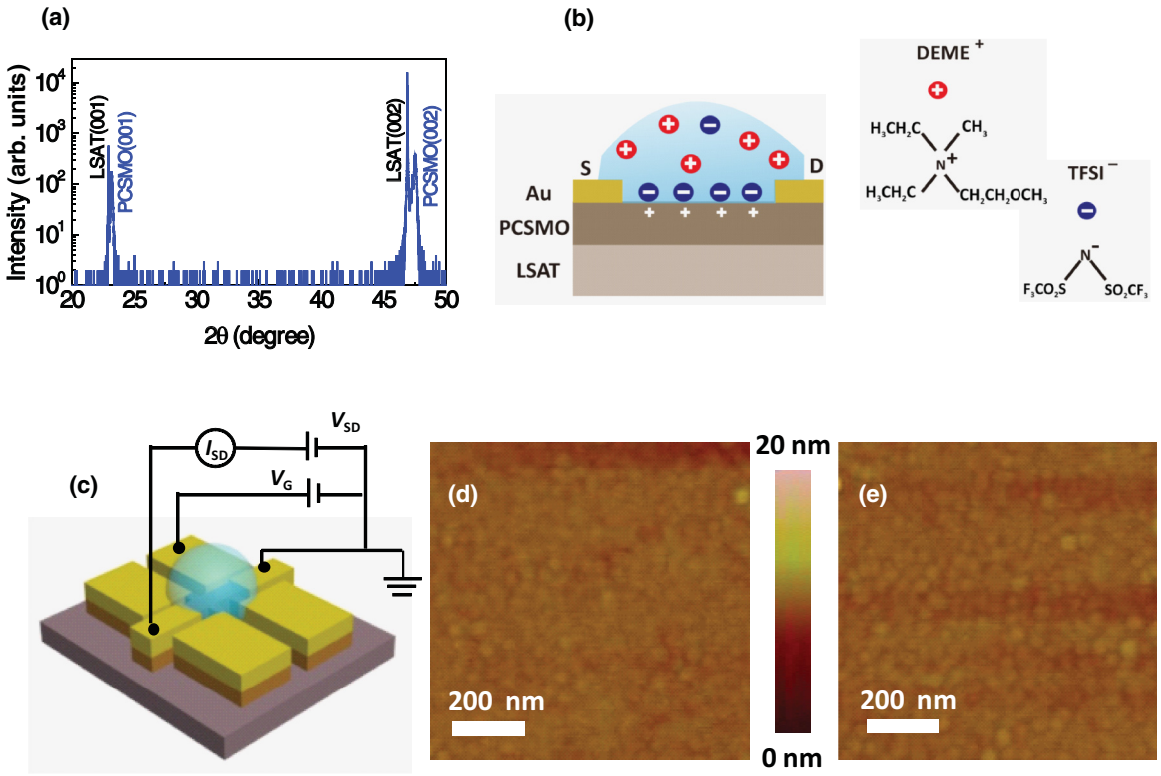

FIG. 1. (Color online) (a) X-ray diffraction θ-2θ scan of the PCSMO film grown on LSAT substrate. (b) Schematic side view of the EDLT. In this particular gate polarity, the PCSMO is in the accumulation state. Also shown are the cationic and ionic molecular components of the electrolyte DEME-TFSI. (c) Schematic of the device, along with the measurement setup. Typical AFM image of the PCSMO film taken (d) right after the PLD growth and (e) after the gating experiments and rinsing off the electrolyte. The scan size of both images is 1×1 μm^2. The RMS roughness measured for (d) and (e) is 0.91 and 1.04 nm, respectively.

by an x-ray diffractometer (SmartLab, Rigaku). The θ-2θ diffraction data taken on the PCSMO film reveal a c-axis orientation with no detectable impurity phase [Fig. 1(a)], and a small tensile strain of ~0.52% was observed. The thickness and the surface roughness of the films were determined by an atomic force microscope (AFM, Dimension V, Veeco). Magnetic measurements of the films were carried out in a superconducting quantum interference device magnetometer (SQUID; MPMS XL-5, Quantum Design).

The schematic of the EDLT is illustrated in Fig. 1(b). The PCSMO films were patterned using photolithography and wet etching. The channel has a typical dimension of 900×300 μm. Au electrodes with a thickness of 70 nm were sputtered through a shadow mask. We used ionic liquid N,N-diethyl-N-methyl-N-(2-methoxyethyl)ammonium bis(trifluoromethylsulphonyl)imide (DEME-TFSI) as the gate dielectric. When a gate bias is applied in an EDLT device, electric double layers are formed at both the gate/ionic liquid and the ionic liquid/channel interfaces [48,50]. When the gate is negatively biased, the migration of the ions in DEME-TFSI leads to the accumulation of holes in the manganite channel, and vice versa, a positive voltage depletes the holes in the channel. Different from the operation mechanism of field effect devices with oxide dielectrics [72], the process of ionic movement in EDLT is capable of creating higher electric fields on the order of megavolts per centimeter at the interface between the electrolyte and the channel [73]. We used silicone paste to confine the ionic liquid covering the channel and a large portion of the gate electrode. Care was taken to make sure that the source and drain contacts remain ohmic during the transport measurements. Au wires were used to contact the electrodes, but they are not in the confined area with ionic liquid in order to maintain measurement stability.

Transport measurements were carried out in a Physical Property Measurement System (PPMS 14T, Quantum Design) with externally connected meters. The measurement setup is schematically illustrated in Fig. 1(c). The gate bias was applied at 230 K, where the ionic liquid is still in the rubber state [48], and maintained for 30 min to allow the polarized ions rearrange their locations. The range of the gate voltage was limited to ± 3 V in order to avoid any electrochemical reaction. During the temperature-dependent transport measurements, the gate bias was kept connected as the device was cooled down. The gate leakage current is in the range of 0.1–5 nA at 230 K and further decreases at lower temperatures. All transport measurements were carried out at a cooling/warming rate of 3 K/min. Typically, the gate voltages were applied in the sequence of -3, -2, -1, 0, $+1$, $+2$, and $+3$ V. We could not determine the exact charge density of the channel, because the Hall effect measurements gave only noisy and unreliable data. Therefore, we calculated the electric field-induced sheet carrier density n_s from the product of the gate voltage and the areal capacitance of the electric double layer C_i, which is typically 10 μF/cm^2 [48]. Gate voltages of 1, 2, and 3 V correspond to modulated sheet carrier densities of 6.25×10^{13}, 1.25×10^{14}, and 1.88×10^{14} cm^{-2}, respectively.

There have been reports on the electrochemical reaction between the ionic liquid and the channel materials [74,75], which may cause experimental artifacts in some cases. To ensure that electrostatic modulation is the dominant effect in our experiments, we used AFM to investigate the surface quality of our channels after the EDLT experiments. As shown in Figs. 1(d) and 1(e), we did not observe any notable change in the surface morphology, and the root-mean-square (RMS) roughness of the film surface remains almost the same after the gating and thermal cycles. In addition, we measured the resistance vs temperature data under the zero gate before and after the gating sequences to make sure that the PCSMO film was not irreversibly damaged during the measurements. Finally, the PPMS chamber was maintained at a pressure of ~7 Torr, which facilitates the measurement reliability since the ionic liquid is quite sensitive to humidity [34].

III. RESULTS AND DISCUSSION

A. Electric field-modulated insulator-metal transitions of the PCSMO film

Figure 2(a) shows the temperature-dependent resistance (R-T) curves for different applied gate voltages measured on a 30 nm thick PCSMO channel (device PCS-A) during both cooling and warming processes. The large thermal hysteresis in the R-T curves is a result of the first-order phase transition between coexisting phases over a range of temperatures [18]. In the pristine state, the resistance peak temperatures T_P are 85 and 98 K for the cooling and warming curves, respectively. Before the application of each gate bias, the device was warmed up to room temperature in order to unfreeze the ionic liquid. Under our measurement conditions, we did

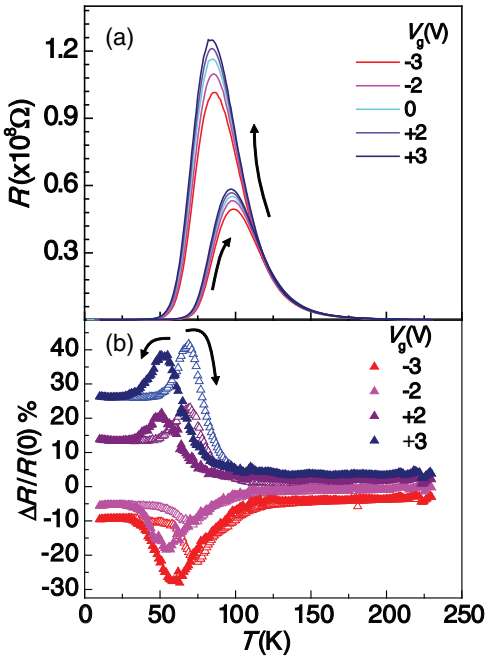

FIG. 2. (Color online) (a) Temperature-dependent resistance of the PCSMO channel (device PCS-A) measured during both warming and cooling (as marked by the arrows) under a series of applied gate voltages (-3, -2, 0, $+2$, and $+3$ V). (b) Corresponding ER vs temperature curves, where ER or $\Delta R/R(0)$ is defined as $\{[R(V_g) - R(0)]/R(0)\}$. The open symbols represent the warming processes, while the filled ones represent the cooling processes; this is also indicated by the arrow directions for $+3$ V gate bias.

not observe any "overshoot" effect of resistance during the repeated thermal cycles [76]. Since PCSMO is a hole-doped manganite, when a negative V_g is applied, holes are injected into the channel, favoring the formation or growth of the FM domains and their percolation. The opposite effect is expected for positive V_g. As shown in Fig. 2(a), when the gate voltage increases from −3 to +3 V, the T_P progressively shifts to lower temperatures and the peak value of resistance increases, which is consistent with the carrier type in the PCSMO channel. Across the whole range of gate voltage, there is a 4-K shift of T_P on cooling and a 2-K shift on warming.

Unless specified otherwise, we define the electroresistance (ER) as the resistance modulation with respect to the zero gate, i.e., $\frac{\Delta R}{R(0)} = \frac{R(V_g)-R(0)}{R(0)}$. As shown in Fig. 2(b), for the cooling cycles, the highest absolute value of ER of 39% was observed ∼50 K for $V_g = +3$ V, whereas the maximum modulation of ∼29% was found at 57 K for $V_g = -3$ V. For the warming cycles, the peak ER is ∼42% at 69 K and ∼23% at 72 K for $V_g = +3$ and −3 V, respectively. In general, ER for positive gate bias is larger than that for negative bias; this trend of polarity dependence is consistent with the report by Dhoot *et al.* [33] on $La_{0.8}Ca_{0.2}MnO_3$ EDLT. The area in the thermal hysteresis decreases by ∼20% on varying the gate bias from +3 to −3 V. The reduction of the thermal hysteresis is similar to the magnetic field effect reported for phase-separated manganites [67].

In previously reported field effect experiments on manganites without macroscopic phase separation, the measured resistance modulation was often discussed in the context of two parallel layers in the channel: One layer near the gate-channel interface with the thickness of approximately the Thomas-Fermi screening length is fully affected by electrostatic doping, whereas the other underlying layer remains unaffected. However, the field-affected layer can extend deeper into the channel if there is any carrier localization effect besides the double-exchange interaction in the manganite channel [39]. Particularly, Jahn-Teller distortion splits the conduction band, and if the thin layer near the gate is converted to be insulating, the electric field will penetrate progressively into the channel [33]. In our case, the PCSMO channel has macroscopic phase separation, which implies an inhomogeneous electric field effect, i.e., the field is screened within the Thomas-Fermi length in the FM metallic domains, similar to the case of double-exchange LSMO [28], whereas the strength of electric field can be expected to be more significant in the CO insulating domains. More discussions on the inhomogeneous nature of the field effect in the region of phase separation are given in later sections.

B. Electric field effect on the small polaron transport

At temperatures above the T_P, the transport in hole-doped manganites is generally of the polaron hopping type as a result of the strong electron-lattice interaction [77]. Depending on the preparation method and the crystalline nature of the manganite films, the polaron hopping transport follows three models; i.e., (i) thermally activated hopping, (ii) variable range hopping, and (iii) small polaron hopping [78]. The existence of polarons significantly affects the transport properties of manganite films and can lead to electrical nonlinearity at the first-order phase

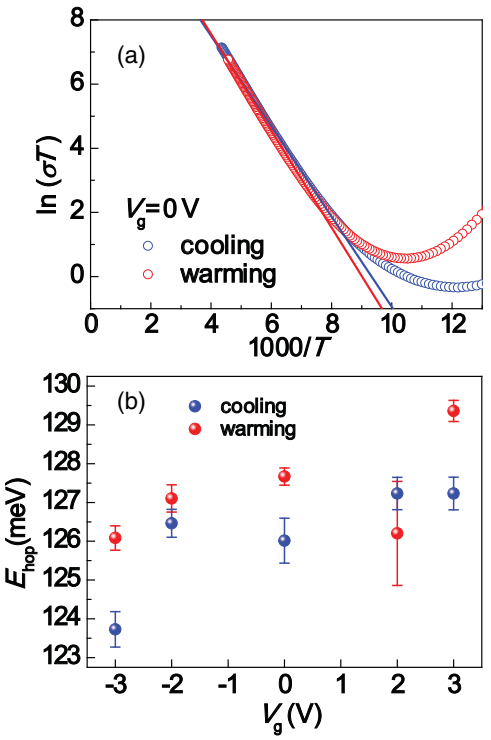

FIG. 3. (Color online) (a) Small polaron fitting to the high-temperature transport data for both the warming and the cooling processes. For clarity, only the zero gate data are shown. (b) Plot of the activation energy $E_{\rm hop}$ as calculated from the fitting to the small polaron model versus the gate voltage.

transition [79]. For our transport data, we found that the small polaron hopping model presents the best fit, which is in line with the good crystalline quality of the epitaxial films used in this paper [78]. The conductivity in the small polaron model has the following temperature dependence [8]:

$$\sigma = \frac{\sigma_0 T_0}{T} \exp\left(-\frac{E_{\rm hop}}{k_B T}\right), \tag{1}$$

where σ_0 is proportional to the product of doping per unit cell and the fractional density of hopping states [24], T_0 is the temperature equivalent of optical phonon energy, and $E_{\rm hop}$ is the activation energy for the polaron hopping, or approximately half of the polaron binding energy [8]. In general, the value of $E_{\rm hop}$ gives a good measure of the Jahn-Teller distortion, which binds the charge carriers in small polarons. As shown in Fig. 3(a), the small polaron model is in good agreement with the transport data in the high-temperature range, i.e., $T > \theta_D/2$, with θ_D being the Debye temperature, while notable deviation emerges at lower temperatures due to band conduction and quantum contributions [80]. The value of θ_D can be estimated as the temperature at which linearity of $\ln(\sigma T)$ vs $1/T$ disappears in the high-temperature region [77]. At the zero gate, the Debye temperatures θ_D were obtained as ∼260 and ∼272 K for the cooling and the warming cycles, respectively. These values are much lower than the Debye temperatures reported for polycrystalline PCSMO samples [77] but comparable to the value determined for $Pr_{0.5}Ca_{0.5}MnO_3$ films [80].

The derived values of activation energies shown in Fig. 3(b) are consistent with the reported results in literature [80]. In addition, we observed an electrostatic modulation of the activation energy of ~3 meV. In the regime of the small polaron transport, the ER is limited below 7%, much smaller than the peak values observed at lower temperatures. Furthermore, we did not observe any obvious hysteresis in the channel conductance versus gate voltage data near room temperature, which is different from the report by Jeong *et al.* on VO_2 EDLT [54]. This indicates that the dynamic oxygen migration at the channel-ionic liquid interface may not be the dominant mechanism underlying the observed transport modulation, although further confirmation is needed in future experiments. It is known that the $Pr_{0.65}(Ca_ySr_{1-y})_{0.35}MnO_3$ series of compounds display a strong electron-phonon interaction characterized by a large polaron coupling constant ($\gamma_p > 4$) and a giant ratio of polaron mass (m_p) to lattice effective mass (m^*) [77]. This strong electron-phonon coupling in the PCSMO channel is likely the reason behind the observed negligible ER in the small polaron transport regime.

C. Electric field effect on the phase separation

At the electrolyte/manganite interface, the electric field created by the electric double layer can be very high due to the short Debye screening length. Considering that the displacement field remains continuous at the electrolyte/manganite interface, we can estimate the strength of the electric field inside the manganite channel. The dielectric constant of ionic liquids is usually in the range of 10–15 [81,82]. However, it is not straightforward to determine the static dielectric constant of the inhomogeneous phase-separated manganite. The dielectric response in such materials undergoes dramatic changes as the electronic phase separation develops [22,83]. In one paper, Kundysa *et al.* [83] used $\varepsilon_i = 35$ and $\varepsilon_m = 55\,000$ as permittivity values in the CO insulating phase and the FM metallic phase, respectively. If we assume the dielectric constant of the ionic liquid as 10 and the electric field as 10^7 V/cm, then the electric field is $\sim 3 \times 10^6$ V/cm in the insulating phase and $\sim 2 \times 10^3$ V/cm in the metallic phase of PCSMO. Clearly, the local electric field in the PCSMO channel varies significantly as a result of the different dielectric constants of separated phases.

We can use a toy model to schematically illustrate the highly inhomogeneous nature of the electric field distribution in the PCSMO channel. In this two-dimensional finite-element model (Fig. 4), we positioned four metal discs with a radius of 5 nm in an insulating host. The conductivities of the insulating matrix and the conductive domains are set as 10^{-2} and 10^5 S/m, respectively. The electric field is screened and negligible in the metallic phase, whereas it is much higher and clearly inhomogeneous in the insulating phase. In particular, the electric field is notably enhanced in the vertical direction near the discs, and the maximum field is 2.4×10^6 V/cm when the nominal applied electric field across the electrodes is 10^6 V/cm. In the phase-separated PCSMO channel studied here, it is quite likely that the local electric field at some geometric sharp protrusions of the metallic domains can produce an electric field high enough to induce the local modification of the insulating phase and even its conversion to the metallic

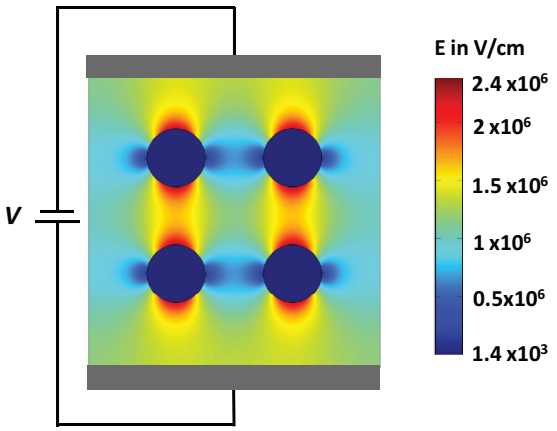

FIG. 4. (Color online) A two-dimensional toy model illustrating the local electric field distribution inside an inhomogeneous media when a voltage is applied across the electrodes. Four metallic spheres with a radius of 5 nm are embedded in an insulating host, and the total thickness of the media between the electrodes is 25 nm, which is close to the actual thickness of the PCSMO film used in our experiments.

phase. However, domains in manganite are quite dynamic, and frozen domains appear only at low temperatures [84,85]. Therefore, the local distribution of electric field in adjacent domains of separated phases and the domain morphology are entangled and evolve concurrently.

We can shed light on the electric field-dependent evolution of different phases and the transport properties using the GEM theory [86,87]. The GEM equation is written as

$$(1-f)\left(\frac{\sigma_I^{1/t}-\sigma_E^{1/t}}{\sigma_I^{1/t}+A\sigma_E^{1/t}}\right)+f\left(\frac{\sigma_M^{1/t}-\sigma_E^{1/t}}{\sigma_M^{1/t}+A\sigma_E^{1/t}}\right)=0, \quad (2)$$

where the effective conductivity (σ_E) of a binary heterogeneous composite is correlated with the conductivities of the randomly distributed metallic (σ_M) and insulating (σ_I) phases. In this equation, f describes the volume fraction of the metallic phase and t is a critical exponent whose value varies from 1.65 to 2 as demanded by universality [87]. The parameter $A = (1 - f_c)/f_c$, with f_c being the percolation threshold. The GEM theory has been demonstrated to describe well the transport properties of phase-separated manganites [88–90], Although the generally accepted three-dimensional value of f_c is 0.16, Kim *et al.* found that $f_c = 0.17$ presents a better fit for $La_{5/8-x}Pr_xCa_{3/8}MnO_3$ (LPCMO) single crystals, whereas even higher values in the range of 0.22–0.24 were found for manganite thin films [88,89,91]. This discrepancy was attributed to both the quasi-two-dimensional nature of the films and the difference of the assumed values of σ_M and σ_I from the actual ones [88].

Since $t = 2$ was found to be suitable for describing manganites [88], Eq. (2) can be rewritten as

$$A\sigma_E + \left(\sigma_M^{1/2} + f\left(\sigma_I^{1/2} - \sigma_M^{1/2}\right) - A\sigma_I^{1/2}\right)\sigma_E^{1/2} - \sigma_I^{1/2}\sigma_M^{1/2} = 0. \quad (3)$$

By assuming the conductivity σ_M of the FM metallic phase is the same as that of $Pr_{0.65}Sr_{0.35}MnO_3$ (PSMO) and σ_I of the CO insulating phase as that of $Pr_{0.65}Ca_{0.35}MnO_3$ (PCMO),

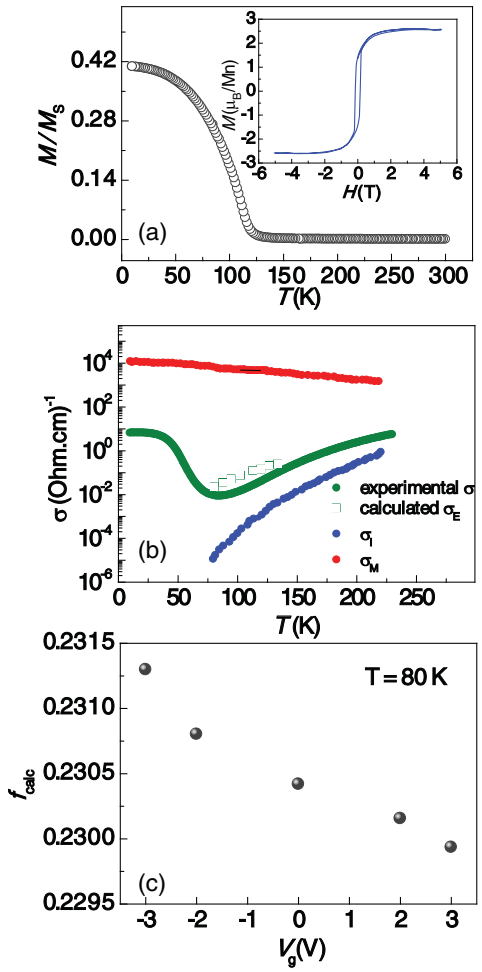

FIG. 5. (Color online) (a) Temperature dependence of the normalized magnetization $\frac{M}{M_S}$, where M was the magnetization of the PCSMO film measured under a magnetic field of 0.1 kOe in a field-cooled process and M_S is the saturation magnetization determined in the 10 K hysteresis loop shown in the inset. (b) Comparison of the measured conductivity of the PCSMO film (green solid circles) with the calculated conductivity (green open squares) based on the GEM theory with the percolation threshold $f_c = 0.24$. Also shown are the conductivity data of PCMO (blue circles) and PSMO (red circles) taken from the paper by Blake *et al.* [64]. (c) Variation of the FM fraction at 80 K calculated from the GEM theory as a function of the applied gate voltage.

we calculated the effective conductivity σ_E of PCSMO. Furthermore, the fraction of the metallic phase f can be estimated from the ratio $\frac{M}{M_S}$, where M and M_S are the measured and the saturation magnetic moments, respectively [92]. We measured the magnetization M of the as-grown sample, and the SQUID data shown in Fig. 5(a) present a clear paramagnetic to FM transition. In addition, according to the M-H curve measured at 10 K, as shown in the inset, M_S is determined as $2.6\mu_B$/Mn. Using the experimentally estimated FM fraction f, henceforth labeled $f_{\rm exp}$, we calculated the effective conductivity σ_E of PCSMO near the percolation transition using Eq. (3). In the calculations, we systematically varied the values of f_c in the range 0.17–0.25 and found that $f_c = 0.24$ led to the closest match of the calculated

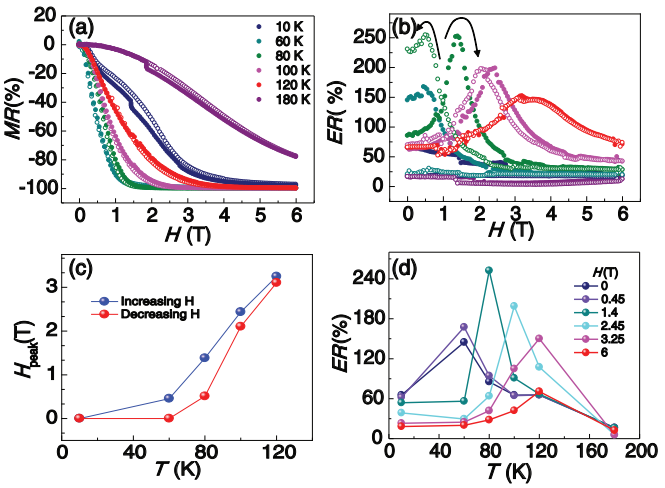

FIG. 6. (Color online) (a) Magnetic field-dependent MR measured on the device PCS-B under the gate bias of −3 V (open circles) and +3 V (filled circles). For clarity, only the data taken on increasing magnetic fields are shown. The small abrupt steps in the data are measurement artifacts. (b) Variation of the ER with the applied magnetic field. Here, ER is defined as $\Delta R/R(-3\ {\rm V}) = \{[R(+3\ {\rm V}) - R(-3\ {\rm V})]/R(-3\ {\rm V})\}$. The filled (open) circles represent the ER data measured on the increasing (decreasing) magnetic field. (c) Plot of the temperature-dependent values of the magnetic field at the peak ER as deduced from Fig. 6(b). (d) Plot of ER vs temperature for different magnetic fields.

conductivities to the experimental data of PCSMO [Fig. 5(b)]. This result is consistent with the previous reports on phase-separated manganites [88,91]. The limited temperature range of the calculated PCSMO conductivity is a result of the high resistance of the PCMO, which could not be measured at temperatures below 75 K. Overall, the calculated PCSMO conductivity values matches the experimental ones, and the slight deviation can be attributed to the uncertainties in the electronic properties of separated phases.

According to the GEM theory, the electric field-induced modulation of σ_E should be correlated with the underlying alteration of the FM fraction f. The modulated σ_E of the PCSMO film at $T = 80$ K can be determined from the transport data shown in Fig. 2. Accordingly, the modulated FM fraction $f_{\rm calc}$ can be obtained from

$$f_{\rm calc} = \frac{\left(\sigma_I^{1/2} - \sigma_E^{1/2}\right)\left(\sigma_M^{1/2} + 3.167\sigma_E^{1/2}\right)}{\sigma_E^{1/2}\left(\sigma_I^{1/2} - \sigma_M^{1/2}\right) + 3.167\sigma_E^{1/2}\left(\sigma_I^{1/2} - \sigma_M^{1/2}\right)}, \quad (4)$$

which is derived from Eq. (2) with $f_c = 0.24$ and $t = 2$. Figure 5(c) shows the gradual increase of the modulated FM fraction $f_{\rm calc}$ at 80 K as the gate voltage changes from +3 to −3 V, and the overall modulation Δf is ∼0.15%.

D. Complementary electric field and magnetic field effects

We further investigated the response of the phase-separated PCSMO channel to simultaneous electric and magnetic fields. A 30-nm PCSMO film (device PCS-B) was prepared under the same conditions as PCS-A. Figure 6(a) shows the data of magnetoresistance (MR), defined as $[R(H) - R(0)]/R(0)$, measured at several temperatures of 10, 60, 80, 100, 120,

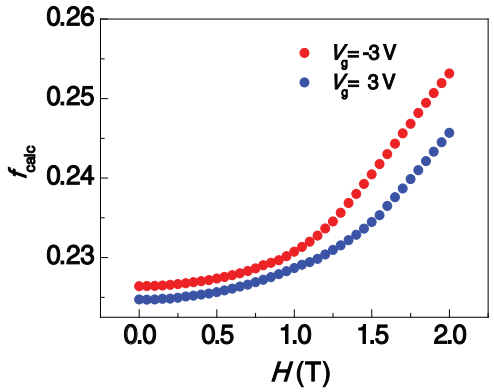

FIG. 7. (Color online) Fraction of the FM phase vs the magnetic field at 80 K for gate voltages of +3 and −3 V as estimated from the GEM theory.

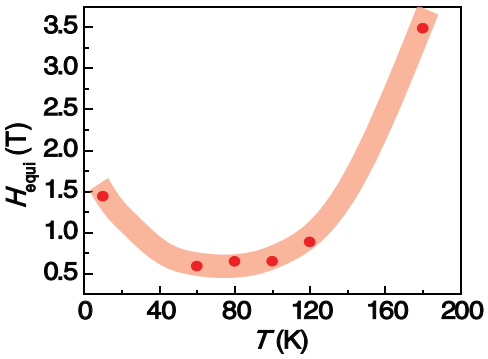

FIG. 8. (Color online) Plot of equivalent magnetic field H_{equi} as a function of temperature. H_{equi} represents the value of a magnetic field, which needs to be introduced on the +3 V gate biased channel in order to produce the same resistance modulation as reversing the gate bias to −3 V.

and 180 K under the gate biases of +3 and −3 V. Figure 6(b) shows the derived ER, which is defined here as $\frac{\Delta R}{R(-3V)} = \frac{R(+3V)-R(-3V)}{R(-3V)}$ as a function of the magnetic field. With the introduction of the magnetic field, the ER reaches the maximum modulation value of ∼250% at 80 K and increasing (decreasing) magnetic field of 1.38 (0.52) T. In comparison, without the magnetic field, the maximum value of $\frac{\Delta R}{R(-3V)}$ is ∼90% at 50 K. The values of the magnetic field H_{peak}, where the ER reaches the maximum, become larger as the temperature increases. Figure 6(c) shows that H_{peak} monotonously increases with temperature. Since the fraction of the FM phase decreases on increasing temperature, a higher magnetic field is naturally needed to maintain the system at the phase-separated state where the ER shows the maximum. Figure 6(d) shows the plot of ER vs temperature at a few representative magnetic fields. Clearly, the applied magnetic field exhibits a significant effect on the temperature-dependent behavior of ER and facilitates the achievement of its maximum values, illustrating the complementary nature of the electric and magnetic field effects.

Out of our chosen set of temperatures, a magnetic field is most effective in boosting the ER at 80 K. We can shed light on the origin of the enhanced ER in the framework of the GEM model. Using the same procedure as the case without a magnetic field, the FM phase faction f_{calc} is determined from the conductivity data by solving Eq. (4). In Fig. 7, we plotted the derived f_{calc} as a function of temperature at gate biases of +3 and −3 V. At 80 K, the ER is highest (∼250%) when a magnetic field of 1.38 T is applied. Under this magnetic field, the change of FM fraction Δf is ∼0.51% when the gate polarity is reversed from +3 to −3 V. In comparison, without any applied magnetic field, Δf is only ∼0.15% when the gate bias changes.

Both the magnetic and the electric field effects are stronger in the phase separation regime, where the competing phases of degenerate energies coexist. Quantitatively, we can compare the ER measured at a zero magnetic field with the MR measured at a fixed gate voltage. We define H_{equi} as the magnetic field that induces the same resistance modulation in the PCSMO channel as the gate voltage of −3 V does. Figure 8 shows the plot of H_{equi} as a function of temperature. At 80 K, where the electric field effect is the highest, H_{equi} is 0.65 T. However, at lower temperatures (<60 K) and higher temperatures (>100 K), the gate voltage of −3 V can substitute significantly higher magnetic fields in modulating the channel resistance. This comparison illustrates the subtle differences between the electric field and the magnetic field on influencing the phase separation and transport properties in PCSMO. In contrast to the isotropic nature of a magnetic field, the local distribution of electric field in the PCSMO channel is expected to be highly inhomogeneous and directional. Future experiments using techniques like Lorentz transmission electron microscopy are warranted to directly probe the evolution of FM and CO domains under the simultaneous stimuli of electric and magnetic fields.

IV. CONCLUSIONS

In this paper, we demonstrated the electric field modulation of transport properties of phase-separated PCSMO in an EDLT. At high temperatures, the electric field effect is rather weak as a result of the small polaron hopping transport with strong electron-phonon coupling. As the measurement temperature lowers and the phase separation sets in, the electric field effect is much enhanced. Furthermore, the electric field effect on such phase-separated manganite exhibits a sensitive dependence on the applied magnetic field, and a maximum ER value of 250% was observed at 80 K when a magnetic field of 1.38 T was applied. By fitting the transport data to the GEM theory, we estimated that the observed resistance modulation is equivalent to an increase of the FM fraction in the PCSMO channel by 0.51%. Our results illustrate the complementary nature of the electric and magnetic field effects in modulating the transport properties of phase-separated manganites. In addition to serving as a powerful tool to unravel the physics of phase separation, EDLT with novel channel materials may open new doors for advancing oxide electronics.

ACKNOWLEDGMENT

We acknowledge the financial support from the Singapore National Research Foundation.

[1] Y. Tokura, Phys. Today **56**, 50 (2003).
[2] C. H. Ahn, J.-M. Triscone, and J. Mannhart, Nature **424**, 1015 (2003).
[3] I. H. Inoue, Semicond. Sci. Technol. **20**, S112 (2005).
[4] J. Chakhalian, A. J. Millis, and J. Rondinelli, Nat. Mater. **11**, 92 (2012).
[5] E. Dagotto, T. Hotta, and A. Moreo, Phys. Rep. **344**, 1 (2001).
[6] Y. Tokura, *Colossal Magnetoresistive Oxides* (Gordon and Breach Science, London, 2000).
[7] A. Moreo, Science **283**, 2034 (1999).
[8] M. B. Salamon and M. Jaime, Rev. Mod. Phys. **73**, 583 (2001).
[9] E. Dagotto, Science **309**, 257 (2005).
[10] Y. Tokura, Science **288**, 462 (2000).
[11] S. Jin, T. H. Tiefel, M. McCormack, R. A. Fastnacht, R. Ramesh, and L. H. Chen, Science **264**, 413 (1994).
[12] Y. Tokura, Rep. Prog. Phys. **69**, 797 (2006).
[13] A. P. Ramirez, J. Phys.: Condens. Matter **9**, 8171 (1997).
[14] J. M. D. Coey, M. Viret, and S. von Molnár, Adv. Phys. **48**, 167 (1999).
[15] M. Fath, S. Freisem, A. A. Menovsky, Y. Tomioka, J. Aarts, and J. A. Mydosh, Science **285**, 1540 (1999).
[16] L. Zhang, C. Israel, A. Biswas, R. L. Greene, and A. de Lozanne, Science **298**, 805 (2002).
[17] E. Dagotto, *Nanoscale Phase Separation and Colossal Magnetoresistance* (Springer-Verlag, Berlin, 2003).
[18] M. Uehara, S. Mori, C. H. Chen, and S. W. Cheong, Nature **399**, 560 (1999).
[19] T. Becker, C. Streng, Y. Luo, V. Moshnyaga, B. Damaschke, N. Shannon, and K. Samwer, Phys. Rev. Lett. **89**, 237203 (2002).
[20] J. Burgy, M. Mayr, V. Martin-Mayor, A. Moreo, and E. Dagotto, Phys. Rev. Lett. **87**, 277202 (2001).
[21] Y. Murakami, H. Kasai, J. J. Kim, S. Mamishin, D. Shindo, S. Mori, and A. Tonomura, Nat. Nanotechnol. **5**, 37 (2009).
[22] Z. Sheng, M. Nakamura, F. Kagawa, M. Kawasaki, and Y. Tokura, Nat. Comm. **3**, 944 (2012).
[23] S. Singh, M. R. Fitzsimmons, T. Lookman, J. D. Thompson, H. Jeen, A. Biswas, M. A. Roldan, and M. Varela, Phys. Rev. Lett. **108**, 077207 (2012).
[24] X. Hong, A. Posadas, A. Lin, and C. H. Ahn, Phys. Rev. B **68**, 134415 (2003).
[25] P. M. Leufke, R. Kruk, R. A. Brand, and H. Hahn, Phys. Rev. B **87**, 094416 (2013).
[26] S. Mathews, Science **276**, 238 (1997).
[27] I. Pallecchi, L. Pellegrino, E. Bellingeri, A. S. Siri, D. Marré, A. Tebano, and G. Balestrino, Phys. Rev. B **78**, 024411 (2008).
[28] X. Hong, A. Posadas, and C. H. Ahn, Appl. Phys. Lett. **86**, 142501 (2005).
[29] C. A. F. Vaz, Y. Segal, J. Hoffman, R. D. Grober, F. J. Walker, and C. H. Ahn, Appl. Phys. Lett. **97**, 042506 (2010).
[30] C. A. F. Vaz, J. Hoffman, Y. Segal, J. W. Reiner, R. D. Grober, Z. Zhang, C. H. Ahn, and F. J. Walker, Phys. Rev. Lett. **104**, 127202 (2010).
[31] S. Brivio, M. Cantoni, D. Petti, and R. Bertacco, J. Appl. Phys. **108**, 113906 (2010).
[32] H. Lu, T. A. George, Y. Wang, I. Ketsman, J. D. Burton, C.-W. Bark, S. Ryu, D. J. Kim, J. Wang, C. Binek, P. A. Dowben, A. Sokolov, C.-B. Eom, E. Y. Tsymbal, and A. Gruverman, Appl. Phys. Lett. **100**, 232904 (2012).
[33] A. S. Dhoot, C. Israel, X. Moya, N. D. Mathur, and R. H. Friend, Phys. Rev. Lett. **102**, 136402 (2009).
[34] P. H. Xiang *et al.*, Adv. Mater. **23**, 5822 (2011).
[35] A. K. Mishra, A. J. Darbandi, P. M. Leufke, R. Kruk, and H. Hahn, J. Appl. Phys. **113**, 033913 (2013).
[36] C. H. Ahn *et al.*, Rev. Mod. Phys. **78**, 1185 (2006).
[37] I. Pallecchi, L. Pellegrino, E. Bellingeri, A. S. Siri, and D. Marré, Phys. Rev. B **71**, 014406 (2005).
[38] T. Wu, S. B. Ogale, J. E. Garrison, B. Nagaraj, A. Biswas, Z. Chen, R. L. Greene, R. Ramesh, T. Venkatesan, and A. J. Millis, Phys. Rev. Lett. **86**, 5998 (2001).
[39] S. B. Ogale, V. Talyansky, C. H. Chen, R. Ramesh, R. L. Greene, and T. Venkatesan, Phys. Rev. Lett. **77**, 1159 (1996).
[40] T. Kanki, Y.-G. Park, H. Tanaka, and T. Kawai, Appl. Phys. Lett. **83**, 4860 (2003).
[41] I. Pallecchi, J. Appl. Phys. **95**, 8079 (2004).
[42] J. T. Ye, S. Inoue, K. Kobayashi, Y. Kasahara, H. T. Yuan, H. Shimotani, and Y. Iwasa, Nat. Mater. **9**, 125 (2010).
[43] K. Ueno, S. Nakamura, H. Shimotani, A. Ohtomo, N. Kimura, T. Nojima, H. Aoki, Y. Iwasa, and M. Kawasaki, Nat. Mater. **7**, 855 (2008).
[44] H. Shimotani, H. Suzuki, K. Ueno, M. Kawasaki, and Y. Iwasa, Appl. Phys. Lett. **92**, 242107 (2008).
[45] H. Shimotani, H. Asanuma, A. Tsukazaki, A. Ohtomo, M. Kawasaki, and Y. Iwasa, Appl. Phys. Lett. **91**, 082106 (2007).
[46] R. Misra, M. McCarthy, and A. F. Hebard, Appl. Phys. Lett. **90**, 052905 (2007).
[47] H. Shimotani, G. Diguet, and Y. Iwasa, Appl. Phys. Lett. **86**, 022104 (2005).
[48] H. Yuan, H. Shimotani, A. Tsukazaki, A. Ohtomo, M. Kawasaki, and Y. Iwasa, Adv. Funct. Mater. **19**, 1046 (2009).
[49] K. Ueno, S. Nakamura, H. Shimotani, H. T. Yuan, N. Kimura, T. Nojima, H. Aoki, Y. Iwasa, and M. Kawasaki, Nat. Nanotechnol. **6**, 408 (2011).
[50] L. Herlogsson, Y.-Y. Noh, N. Zhao, X. Crispin, H. Sirringhaus, and M. Berggren, Adv. Mater. **20**, 4708 (2008).
[51] A. T. Bollinger, G. Dubuis, J. Yoon, D. Pavuna, J. Misewich, and I. Bozovic, Nature **472**, 458 (2011).
[52] J. T. Ye, Y. J. Zhang, R. Akashi, M. S. Bahramy, R. Arita, and Y. Iwasa, Science **338**, 1193 (2012).
[53] M. Nakano, K. Shibuya, D. Okuyama, T. Hatano, S. Ono, M. Kawasaki, Y. Iwasa, and Y. Tokura, Nature **487**, 459 (2012).
[54] J. Jeong, N. Aetukuri, T. Graf, T. D. Schladt, M. G. Samant, and S. S. P. Parkin, Science **339**, 1402 (2013).
[55] R. Scherwitzl, P. Zubko, I. G. Lezama, S. Ono, A. F. Morpurgo, G. Catalan, and J.-M. Triscone, Adv. Mater. **22**, 5517 (2010).
[56] Y. Yamada *et al.*, Science **332**, 1065 (2011).
[57] Y. Li, R. Deng, W. Lin, Y. Tian, H. Peng, J. Yi, B. Yao, and T. Wu, Phys. Rev. B **87**, 155151 (2013).
[58] S. Asanuma *et al.*, Appl. Phys. Lett. **97**, 142110 (2010).
[59] P. H. Xiang, S. Asanuma, H. Yamada, H. Sato, I. H. Inoue, H. Akoh, A. Sawa, M. Kawasaki, and Y. Iwasa, Adv. Mater. **25**, 2158 (2013).
[60] X. Leng, J. Garcia-Barriocanal, S. Bose, Y. Lee, and A. M. Goldman, Phys. Rev. Lett. **107**, 027001 (2011).
[61] C. Thiele, K. Dörr, L. Schultz, E. Beyreuther, and W. M. Lin, Appl. Phys. Lett. **87**, 162512 (2005).
[62] R. K. Zheng, Y. Wang, H. L. W. Chan, C. L. Choy, and H. S. Luo, Appl. Phys. Lett. **90**, 152904 (2007).
[63] K. Dörr and C. Thiele, Phys. Status Solidi B **243**, 21 (2006).
[64] G. R. Blake, L. Chapon, P. G. Radaelli, D. N. Argyriou, M. J. Gutmann, and J. F. Mitchell, Phys. Rev. B **66**, 144412 (2002).

[65] T. Wu and J. F. Mitchell, Phys. Rev. B **74**, 214423 (2006).
[66] T. Wu and J. F. Mitchell, Appl. Phys. Lett. **86**, 062502 (2005).
[67] T. Z. Ward, S. Liang, K. Fuchigami, L. F. Yin, E. Dagotto, E. W. Plummer, and J. Shen, Phys. Rev. Lett. **100**, 247204 (2008).
[68] H.-Y. Zhai, J. X. Ma, D. T. Gillaspie, X. G. Zhang, T. Z. Ward, E. W. Plummer, and J. Shen, Phys. Rev. Lett. **97**, 167201 (2006).
[69] J. F. Ding, K. X. Jin, Z. Zhang, and T. Wu, Appl. Phys. Lett. **100**, 062402 (2012).
[70] M. Tokunaga, Y. Tokunaga, and T. Tamegai, Phys. Rev. Lett. **93**, 037203 (2004).
[71] T. Z. Ward *et al*., Phys. Rev. Lett. **102**, 087201 (2009).
[72] B. Nagaraj, T. Wu, S. B. Ogale, T. Venkatesan, and R. Ramesh, J. Electroceram. **8**, 233 (2002).
[73] R. Kotz and M. Carlen, Electrochim. Acta **45**, 2483 (2000).
[74] H. Yuan, H. Shimotani, J. Ye, S. Yoon, H. Aliah, A. Tsukazaki, M. Kawasaki, and Y. Iwasa, J. Am. Chem. Soc. **132**, 18402 (2010).
[75] S. Thiemann, S. Sachnov, S. Porscha, P. Wasserscheid, and J. Zaumseil, J. Phys. Chem. C **116**, 13536 (2012).
[76] D. Khomskii and L. Khomskii, Phys. Rev. B **67**, 052406 (2003).
[77] S. Mollah, H. L. Huang, H. D. Yang, S. Pal, S. Taran, and B. K. Chaudhuri, J. Magn. Magn. Mater. **284**, 383 (2004).
[78] M. Ziese and C. Srinitiwarawong, Phys. Rev. B **58**, 11519 (1998).
[79] V. Moshnyaga, K. Gehrke, O. I. Lebedev, L. Sudheendra, A. Belenchuk, S. Raabe, O. Shapoval, J. Verbeeck, G. Van Tendeloo, and K. Samwer, Phys. Rev. B **79**, 134413 (2009).
[80] C. Jooss, L. Wu, T. Beetz, R. F. Klie, M. Beleggia, M. A. Schofield, S. Schramm, J. Hoffmann, and Y. Zhu, Proc. Natl. Acad. Sci. USA **104**, 13597 (2007).
[81] J. P. Hallett and T. Welton, Chem. Rev. **111**, 3508 (2011).
[82] C. Wakai, A. Oleinikova, M. Ott, and H. Weingartner, J. Phys. Chem. B **109**, 17028 (2005).
[83] B. Kundys, N. Bellido, C. Martin, and C. Simon, Eur. Phys. J. B **52**, 199 (2006).
[84] L. Ghivelder and F. Parisi, Phys. Rev. B **71**, 184425 (2005).
[85] J. Sacanell, F. Parisi, J. C. P. Campoy, and L. Ghivelder, Phys. Rev. B **73**, 014403 (2006).
[86] D. S. McLachlan, J. Phys. C Solid State **20**, 865 (1987).
[87] D. S. McLachlan, M. Blaszkiewicz, and R. E. Newnham, J. Am. Ceram. Soc. **73**, 2187 (1990).
[88] T. Wu, S. B. Ogale, S. R. Shinde, A. Biswas, T. Polletto, R. L. Greene, T. Venkatesan, and A. J. Millis, J. Appl. Phys. **93**, 5507 (2003).
[89] K. H. Kim, M. Uehara, C. Hess, P. A. Sharma, and S.-W. Cheong, Phys. Rev. Lett. **84**, 2961 (2000).
[90] V. Markovich, I. Fita, R. Puzniak, A. Wisniewski, K. Suzuki, J. W. Cochrane, Y. Yuzhelevskii, Y. M. Mukovskii, and G. Gorodetsky, Phys. Rev. B **71**, 224409 (2005).
[91] V. Markovich, E. S. Vlakhov, Y. Yuzhelevskii, B. Blagoev, K. A. Nenkov, and G. Gorodetsky, Phys. Rev. B **72**, 134414 (2005).
[92] M. Jaime, P. Lin, S. H. Chun, M. B. Salamon, P. Dorsey, and M. Rubinstein, Phys. Rev. B. **60**, 1028 (1999).